

Figure S1. Antigen encounter triggers nucleation of actin foci and cellular symmetry. Related to Figure 1. APS with indicated ligands were incubated with T cells for 2min, fixed, stained with phalloidin-Alexa488 and imaged using SIM. The graph shows quantification of cell shape in cells. Scale bar, 5µm. P values ***<0.0001, as measured using Mann-Whitney test.

Figure S2. The aspect ratio (AR) reports on synaptic interface elongation associated with radial interface symmetry breaking. Related to Figure 1. (A) Interference reflection microscopy (IRM) of mouse CD4⁺ T cells (T cells) shows that significant changes in shape and motility of T cell contact interfaces can be recorded within a time span of 2min, between their 'arrested' (sedentary) and 'motile' states. The motile or arrested cells were manually identified in the time-lapse images, 20 min post their initial contact with APS, and associated mean aspect ratios and speed were analyzed over a time span of 2 min. The graph shows an average value of speed or AR spanning 2 min. (B) Alteration in speed and shape measured at the population level during synapse breaking. Snapshots of T cells from time-lapse IRM imaging after seeding on APS, with overlaid center-of-mass tracks over time (in color). Shown at right are the speed and aspect ratios calculated within a 2 min window of observation at 5 min or 20 min post cell seeding; points are individual cells. Scale bar, 5µm. P values ***<0.0001, as measured using Mann-Whitney test.

Figure S3. (A-B) Image processing scheme utilized to extract and quantify foci on per cell basis. Related to Figure 1. The images show 2D F-actin intensity as marked by phalloidin staining (top images), or a 3D view of spatial distribution of intensities in the phalloidin images (bottom images). To process the raw images for extracting foci intensities from overall F-actin signal, a Gaussian mask was generated by using a 1.6µm X 1.6µm rolling window, as optimized previously¹. Subtraction of the mask image from the raw image generated a processed image that could be quantified to measure the average intensity contributed by the foci. Note that while this method reliably identifies the foci in raw images and reduces intensity contribution from the non-foci uniform lamellar area, the peripheral lamellipodial network still contributes a background of ~35% to the total foci intensity, regardless of the presence of profuse foci in arrested synapse, or their visible reduction in the motile phase.

Figure S4. Calcium sequestration using BAPTA does not predispose cells to synapse breaking. Related to Figure 1. T cells were incubated with APS for 5 min or for 20 min, along with vehicle control or BAPTA and EGTA in the last 10 min of incubation, fixed, stained with phalloidin-Alexa568 and anti-Talin antibody, imaged using SIM (A). Note

that the BAPTA-treated cells retain symmetry more than the control cells, and display significantly more foci, even when they have comparable talin recruitment at the synapse (B). P values; $** \leq 0.005$, n.s. for talin= 0.067; n.s. for total actin= 0.22. P values for the comparisons not shown >0.05 as measured using Mann-Whitney test. The points in the plots are the values obtained from individual cells normalized to mean of 5' values.

Figure S5. Synapse symmetry breaking in T cells activated using BMDCs. OTII T cells were activated on OVA peptide-loaded BMDCs for the indicated time points, fixed, stained and imaged using spinning disc confocal microscopy. The images show maximum intensity projection of the area encompassing T cell-BMDC contacts (A), the arrows in left panels show synapse sites, and the arrows in right panels show foci sites within a synapse. P values in quantifications in (B), $*** < 0.0001$; $**$ in pWASP= 0.006; $**$ in AR= 0.001; p values for the comparisons not shown >0.05 , as measured using Mann-Whitney test. The points in the bottom left plot are the values obtained from individual cells normalized to mean of 5' values. (C) Shows the actin foci in a 5' synapse formed at the pericellular edge of BMDC.

Figure S6. Endogenous pCasL serves as a reliable mechanotransduction marker in T cells. Related to Figure 3. (A) A schematic of mechanosensitive CasL phosphorylation in T cells. CasL is recruited to the signaling TCR clusters via LCK via its Src kinase Binding domain (SB), and interacts with the F-actin cytoskeleton and adhesion complex binding proteins such as FAK via its SH3 domain. Mechanical tension created due to actin polymerization and actomyosin contraction at the foci sites leads to conformational changes in CasL, exposing tyrosine motifs in its substrate domain. These tyrosine residues are phosphorylated by the local Src-Family kinases, and could be immunolabelled to assess TCR-proximal actin cytoskeletal strains. (B, C) Colocalization index of foci and pCasL shows a high degree of association (left plot in C), and correlation with foci intensity per cell (right plot in C). (D) pCasL levels are sensitive to broad actin cytoskeletal perturbation. T cells from WT mice were treated with Latrunculin A (LatA), or left untreated, during incubation with substrate. Cells were subsequently fixed and processed for immunostaining and imaged using TIRF microscopy. $** = 0.001$ for pCasL. (E) WT T cells show reduced pCasL in polarized synapses. $p < 0.0001$, as measured using Mann-Whitney test. (F) The recruitment of CasL to the synapse are not reduced in WASP-/- T cells. The points in (D-F) are the values obtained from individual cells normalized to mean of WT (D) or 5' (E) values.

Figure S7. (A-B) WASP overexpression restores actin foci and synapse symmetry. (A) Western blotting of endogenous WASP and overexpressed GFP-WASP in T cells after 20 min incubation on anti-CD3/ICAM-1-coated substrates. The numbers in the graphs represent ratios of WASP: actin band intensities, normalized to the control lane. (B) TIRF imaging of wild type and GFP-WASP-overexpressing T cells incubated with anti-CD3/ICAM-1 substrates, for analysis of AR, actin, and pCasL levels. Fluorescence levels normalized to mean values at 5 min; points represent data from individual cells. **, $p = 0.009$; ***, $p < 0.0001$; for n.s., $p < 0.05$ using Mann-Whitney test. (C) Synapse symmetry breaking is associated with loss of foci and active WASP in human primary CD4⁺ T cells. Freshly isolated human CD4⁺ T cells were activated using the substrates for indicated durations, fixed, stained and imaged using TIRF microscopy. In the graph, p values ***, $p < 0.001$; p values for n.s. or the comparisons not shown > 0.05 , as measured using Mann-Whitney test. The points in the left plot in (C) are the values obtained from individual cells normalized to mean of 5' values in each case.

Figure S8. Related to Figure 3. (A) Initial adhesion and spreading kinetics is comparable in WASP^{-/-} and WT T cells activated on the antigenic surface, WASP^{-/-} cells however show interface elongation at earlier time point (~3 min) than the WT cells. T cells were incubated with substrates on a temperature-controlled microscope stage, imaged live using TIRFM (Movie 5), and analyzed for spreading and shape elongation. (B) Synapse breaking in WT and WASP^{-/-} cells. Images are snapshots of T cells from time-lapse IRM imaging after seeding on APS, with overlaid center-of-mass tracks over time (in color); the graph showed measured speed.

Figure S9. Related to Figure 3. (A) TCR engagement-induced phosphorylation of early signaling molecules Zap70, SLP76, LAT. The points in the plots represent values obtained from individual cells normalized to the mean of 'WT' values. (B, C) Colocalization of foci (derived from Phalloidin- Alexa 568 images) with phospho-Zap70 (B), and with phospho-PLC γ 1 (C) is substantially reduced in late (15') synapses of WT T cells. P values n.s. > 0.05 ; ***, < 0.001 ; **, $= 0.01$, as measured using Mann-Whitney test.

Figure S10. Related to Figure 3. (A) SIM imaging of 2 min WASP^{-/-} T cells synapses shows that these cells are able to initially generate radially symmetric ICAM-1 ring in their synapse. Cells were incubated with lipid bilayers reconstituted with anti-CD3 and ICAM1-Cy5, fixed, stained for F-actin and talin and visualized using SIM. (B) Integrin hyperactivation does not rescue symmetry defects in WASP^{-/-} T cells. WT or WASP^{-/-} T cells were incubated with APS in the presence or absence of 0.5mM MnCl₂ for 5 min, fixed and processed for talin, pCasL and F-actin

(phalloidin-Alexa 568) visualization, and imaged using TIRFM. P values ***<0.001; *= 0.01; n.s. >0.05, as measured using Mann-Whitney test.

Figure S11. Related to Figure 3. Intracellular calcium flux is not enough to revert asymmetry in WASP^{-/-} cells. T cells from WT or WASP^{-/-} mice were incubated with APS in the presence of DMSO or 1μM Thapsigargin (Thapsi) for 5'. The cells were then fixed and processed for talin, pCasL and F-actin (Phalloidin-Alexa 568) visualization. Note that while Thapsigargin treatment is unable to restore symmetry in WASP^{-/-} cells (A, B), it induces downregulation of talin in both WT and WASP^{-/-} T cells (quantification in B). P values, ***<0.0001; *= 0.01 and 0.02 respectively, as measured using Mann-Whitney test. The points in the plots are the values obtained from individual cells normalized to mean of 'WT' in each case.

Figure S12. Related to Figure 3. (A) pCasL-enriched actin foci in antigen-specific cell-cell conjugate setting. BMDCs loaded with OTII peptide were incubated with mouse WT or WASP^{-/-} OTII transgenic CD4⁺T cells for 5', fixed and processed for SIM imaging. The image shows maximum intensity projection from 2μm depth of the synaptic area of a single T cell, marked by a white box. The graph on the right shows actin foci and F-actin (phalloidin-Alexa568) and pCasL intensity, or AR, measured at the synapse. The points in the plots are the values obtained from individual cells normalized to mean of 'WT' in each case. P values, *= 0.01; **= 0.009; ***<0.0001. (B) Representative Total Internal Reflection Fluorescence microscopy (TIRF) images of primary human CD4⁺ T cells isolated from healthy individuals or WAS patients and activated for 5' on APS. Graph on the right shows quantification of actin foci, pCasL, and cell AR normalized to mean values of control healthy individual cells. P values ***< 0.001, as measured using Mann-Whitney test.

Figure S13. Related to Figure 3. Transient reduction of WASP levels in human cells elicits defects comparable to those observed in murine WASP^{-/-} T cells. (A) Human CD4⁺ T cells transduced with control lentivirus or with lentivirus delivering WASP shRNA (as described in Kumari et. al., eLife, 2015), seeded onto superantigen-loaded HUVEC cells for 5', then fixed, stained for actin (phalloidin-Alexa568) and pCasL, and imaged using a spinning disc confocal microscope. P values *** <0.0001, as measured using Mann-Whitney test. The points in the top plots are values obtained from individual cells normalized to mean of 'control' case. (B) Foci polymerization role of WASP underlies its mechanical tension-generating activity. Human CD4⁺T cells were transfected with human WT WASP-GFP, WASPΔC or with WASP shRNA (shR)-transducing lentiviral particles. The data shows that the WASP shR and

WASPΔC reduce foci and pCasL at the synapse to a similar extent. The remaining foci in the cells in the shR and WASPΔC are contributed by APC cytoskeletal features underneath the synapse, which are quantified along with foci by our foci extraction algorithm outlined in Figure S3. The bars in the graph show the mean values normalized to the mean of 'WT' in each case.

Figure S14. Related to Figure 4. (A) Endogenous myosinII distribution at the synapse in the stable (upper panels) and broken phase (lower panels) of synapse, as visualized using SIM. Arrows shows the location of myosin puncta juxtaposed with the actin foci (derived from phalloidin-Alexa658 images). Note that the local molecular organization inside foci appear different between our simulations and experiments- simulations show that myosinII localizes at the foci, while the immunostaining here shows that myosinII localizes to the inter-foci areas. Future computational studies involving additional higher order molecular level interactions are needed to determine the origins of the intra-foci architecture. (B) F-actin architecture and stresses on a curved surface resemble those on the flat surface. Simulation on a curved surface of radius $9.6\mu\text{m}$ shows that F-actin localizes in the inter-foci regions, away from the periphery, similar to that on a flat substrate in Figure 4.

Figure S15. Related to Figure 5. Azido-blebb. treatment itself, in the absence of photoactivation, does not influence symmetry breaking. T cells were allowed to form synapse on APS for 5 min, were then treated with DMSO vehicle (control) or with $5\mu\text{M}$ Azido-blebb. On the substrate. Cells were then imaged and analyzed as described in Figure 5H.

Videos:

Video S1. Related to Figure 1. Six different examples of cells breaking their sedentary primary contacts and showing interface shape elongation and a shift in motility, imaged using IRM, indicate that rapid shape transitions can be quantified with 2 min of time duration.

Video S2. Related to Figure 1. IRM live imaging of T cells using reveals a significant shift away from the primary synapse site within 20 min of APS encounter. The images were negatively contrasted to identify cell positions and better highlight individual cell boundaries using automated cell outlining (object identification) routine in ImageJ.

The residual material left by the T cells on the primary contact site is reminiscent of membrane fragments, as described in⁵.

Video S3. Related to Figure 2. LLSM live imaging of mouse T cell synapse expressing LifeAct-GFP, during transition to the motile phase.

Video S4. Related to Figure 2. LifeAct-GFP expressing WT or WASP^{-/-} T cells reveal differential dynamics of lamella vs. the foci. Cells were allowed to attach to the APS for 5min (t=0 in the movie), and then imaged using TIRFM.

Video S5. Related to Figure 3. WASP^{-/-} cells break contact symmetry faster than the WT T cells. T cells isolated from WT or WASP^{-/-} mice were imaged live using IRM for 10 min at 3 frames/min. The images were negatively contrasted for automated boundary identification (Movie 8; see 'Methods') and tracked for the center of mass movement. Bottom panels represent the cell traces overlaid in top panels.

Videos S6-9. Related to Figure 4. Simulations showing evolution of F-actin network in the WT (whole stable synapse, Movie 6; magnified view of cytoskeletal dynamics around foci, Movie 7), WASP^{-/-} (predisposed to breaking, Movie 8), and a WT synapse transitioning into polarized state (Movie 9), soon after the initial antigen encounter and spreading. Each movie represents a synapse as a rectangular simulation space, based on the scheme presented in Figure 4A. Note that WT synapse in Movie 9 loses established symmetry the instant WASP is removed from the simulation.

Video S10. Related to Figure 5. LLSM imaging of cells treated with CK666 show a loss of foci and altered actin dynamics in the synapse similar to that in the case of WASP^{-/-} cells.

Video S11. Related to Figure 5. Simulation showing the effect of localized myosin perturbation on F-actin network connectivity on the tension within the synapse. The simulation scheme described in Figure 4A was used to create F-actin distribution in synapse, where a perturbation in myosinII was introduced in a rectangular shaped subsynaptic region, shortly after the synapse was established (corresponding to the image shown in Figure 5h).

Video S12. Related to Figure 6. Control or Azidoblebb.-treated cells, corresponding to the images shown in Figure 4h (photoactivable inhibition of myosinII).

Figure S1

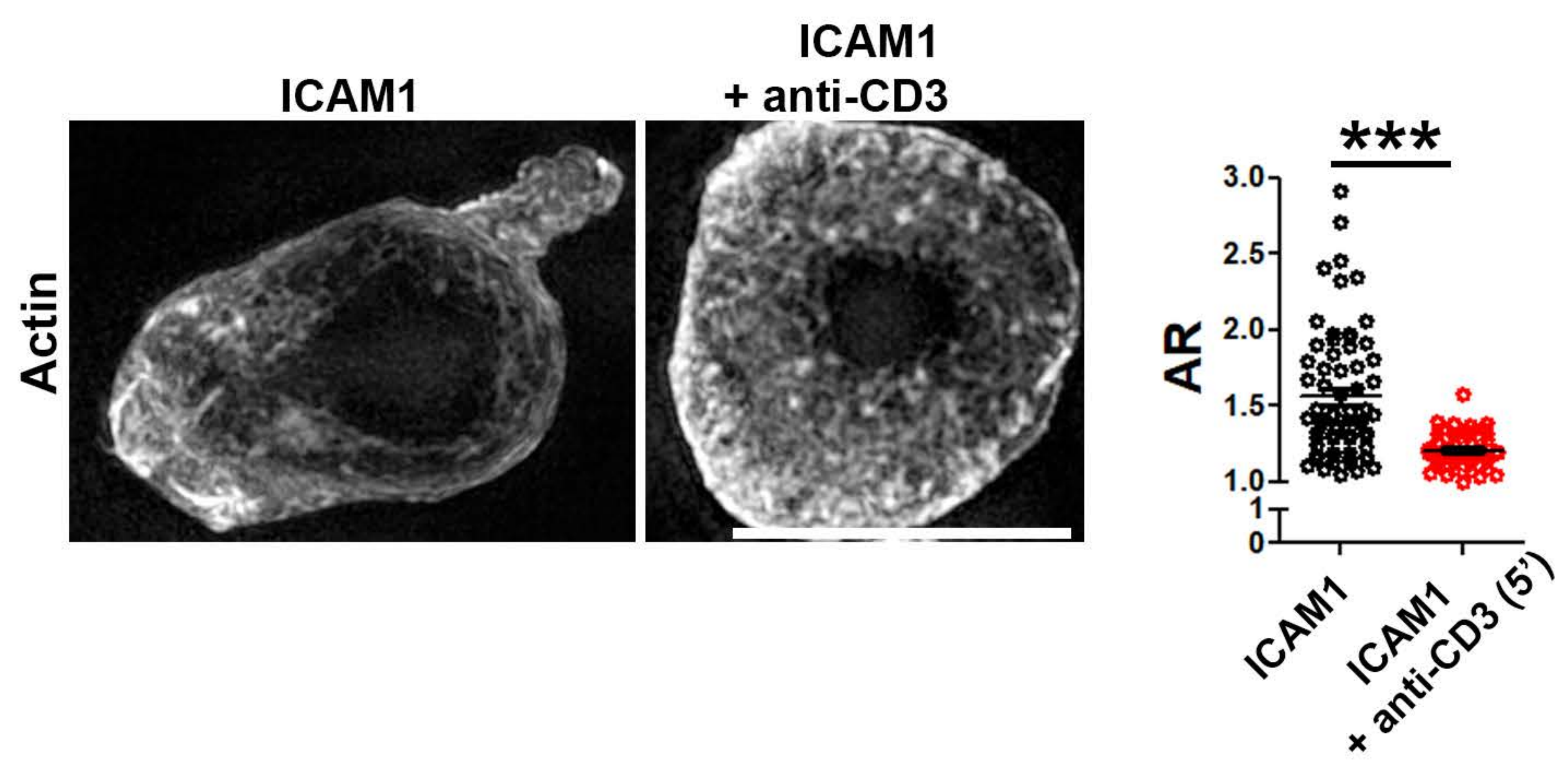
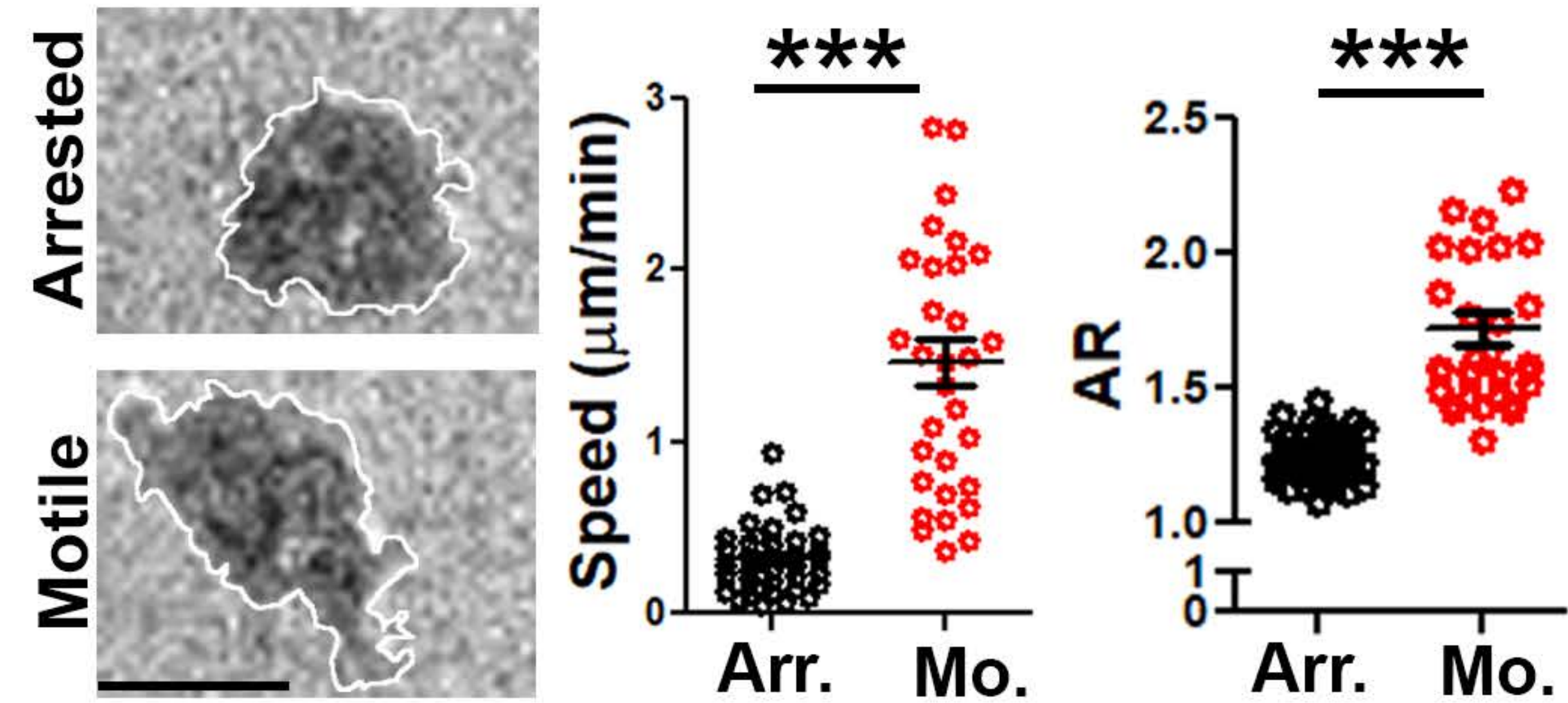


Figure S2

A



B

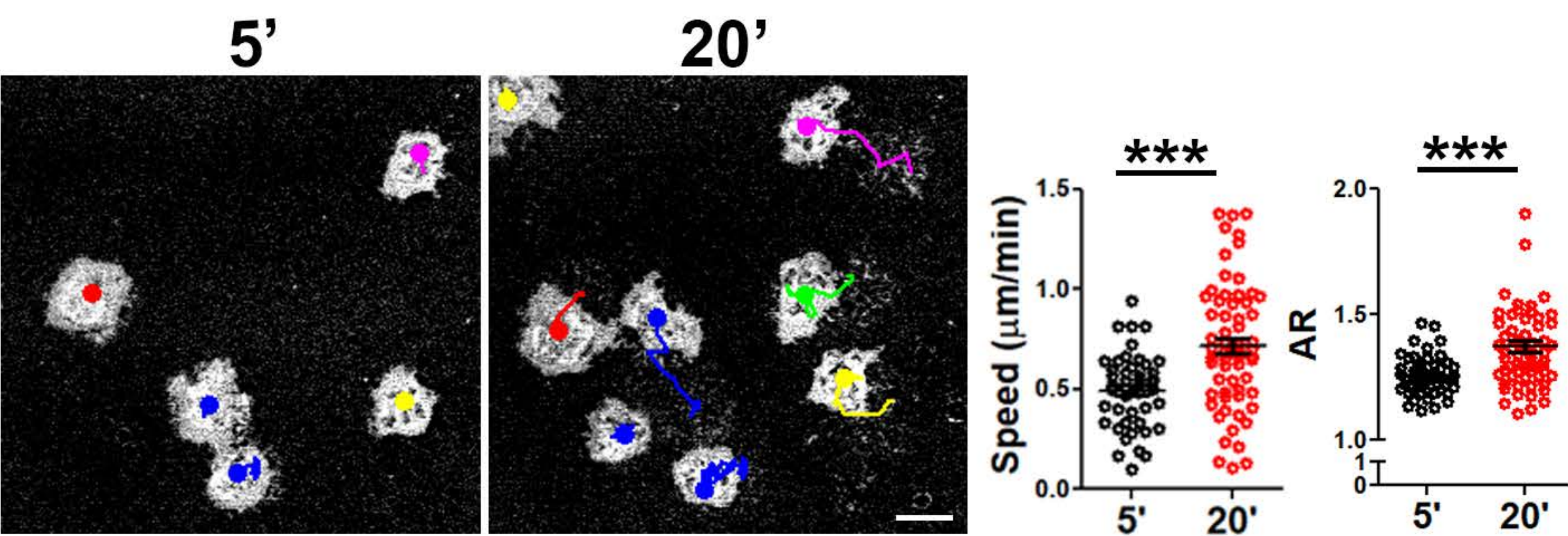


Figure S3

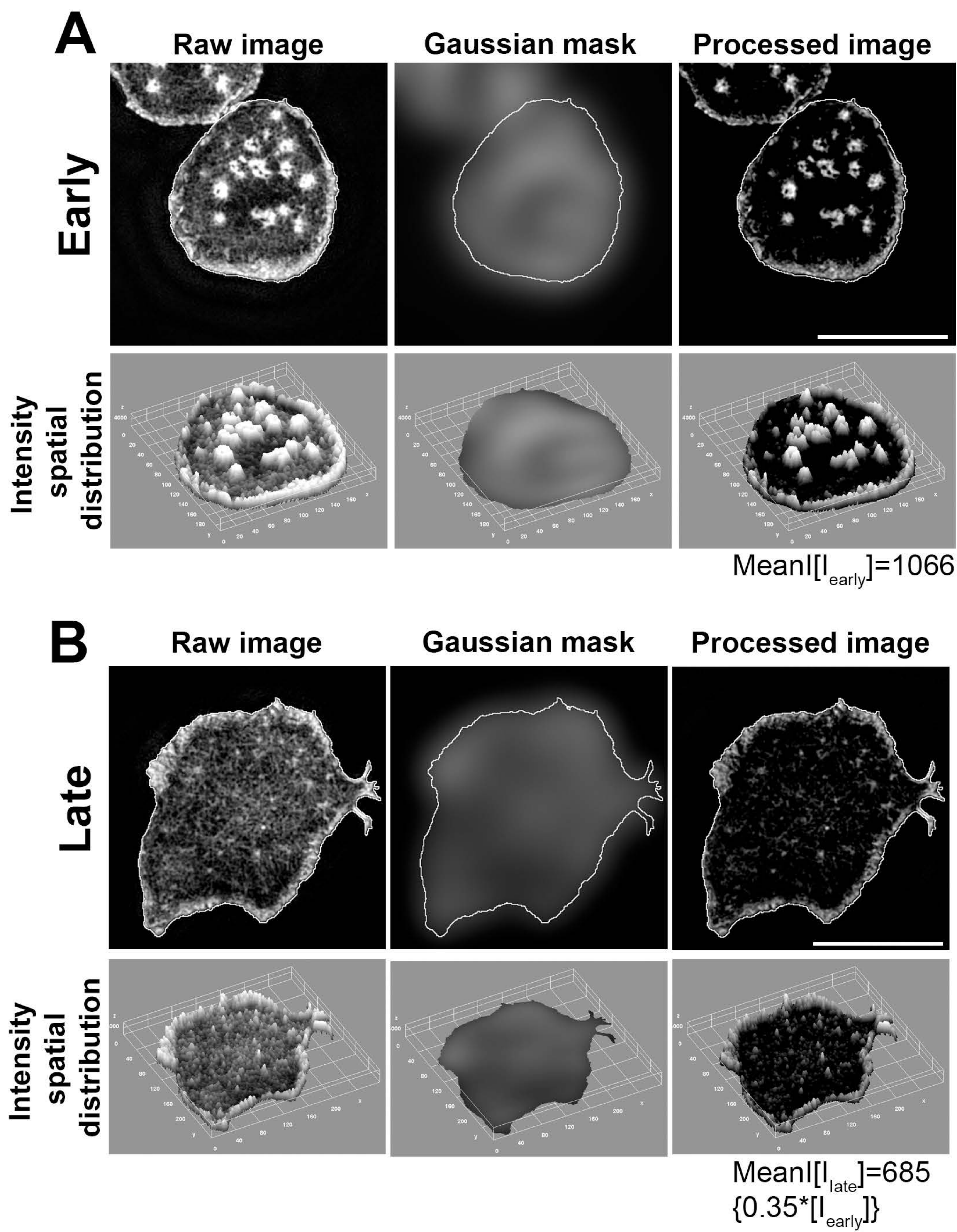


Figure S4

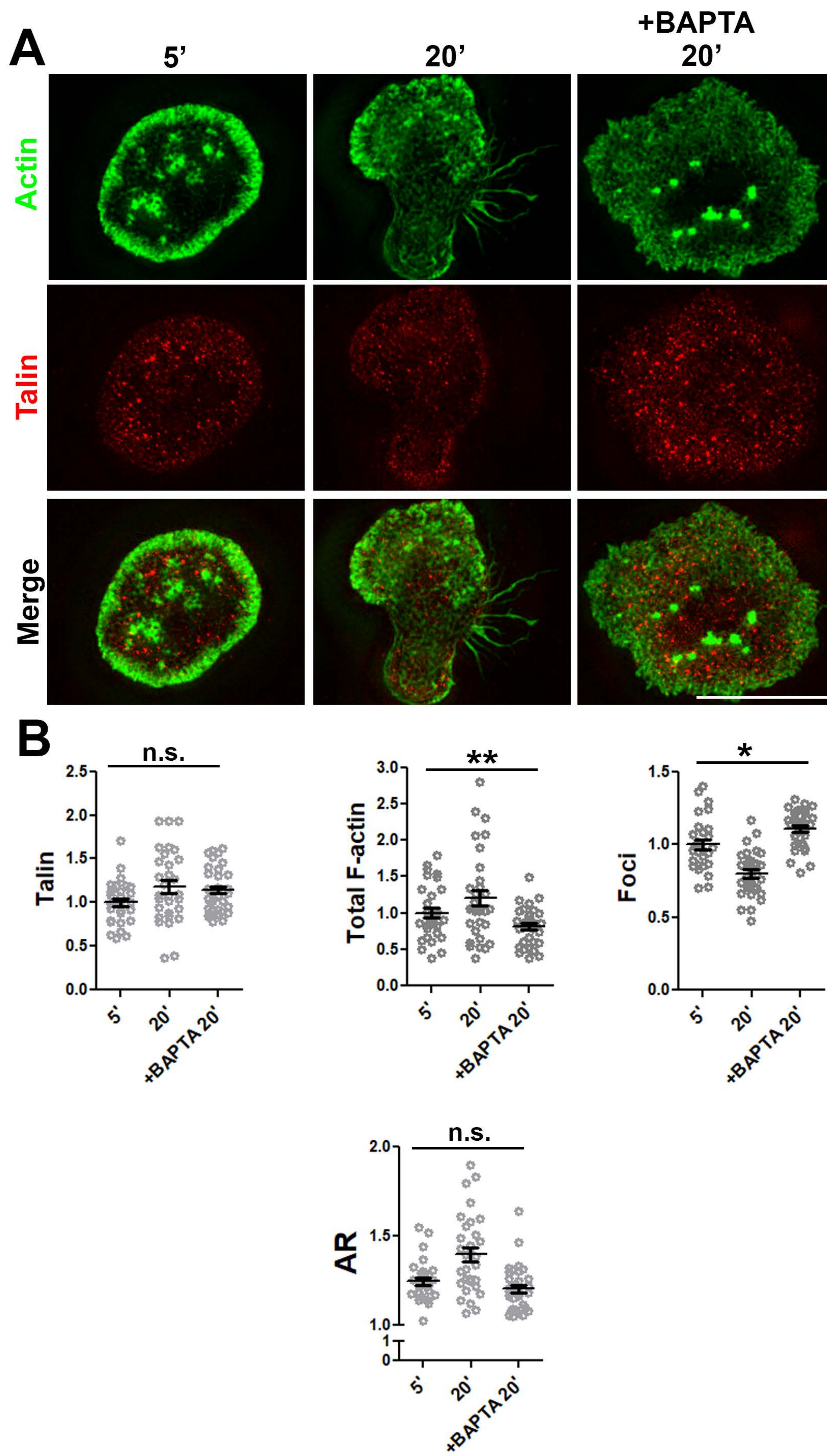


Figure S5

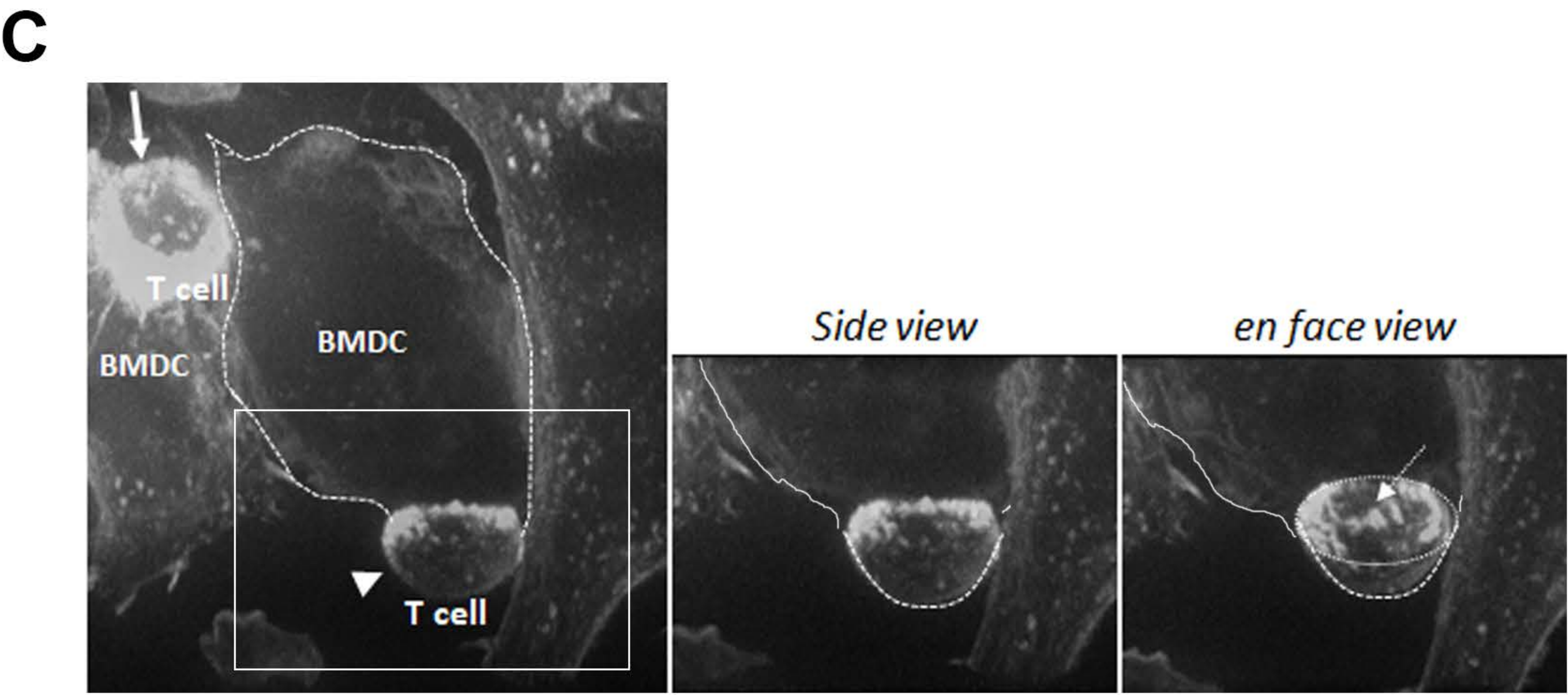
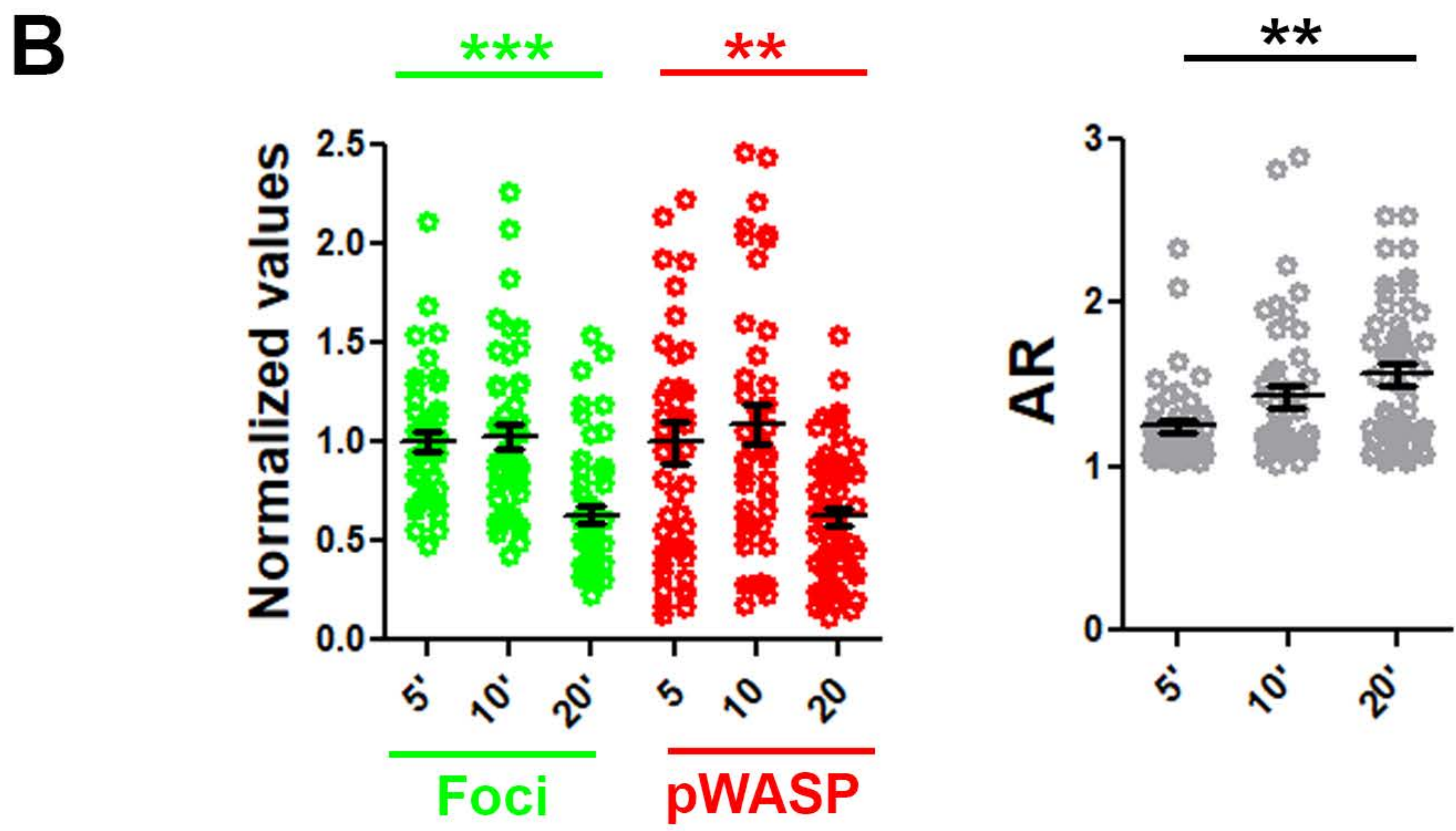
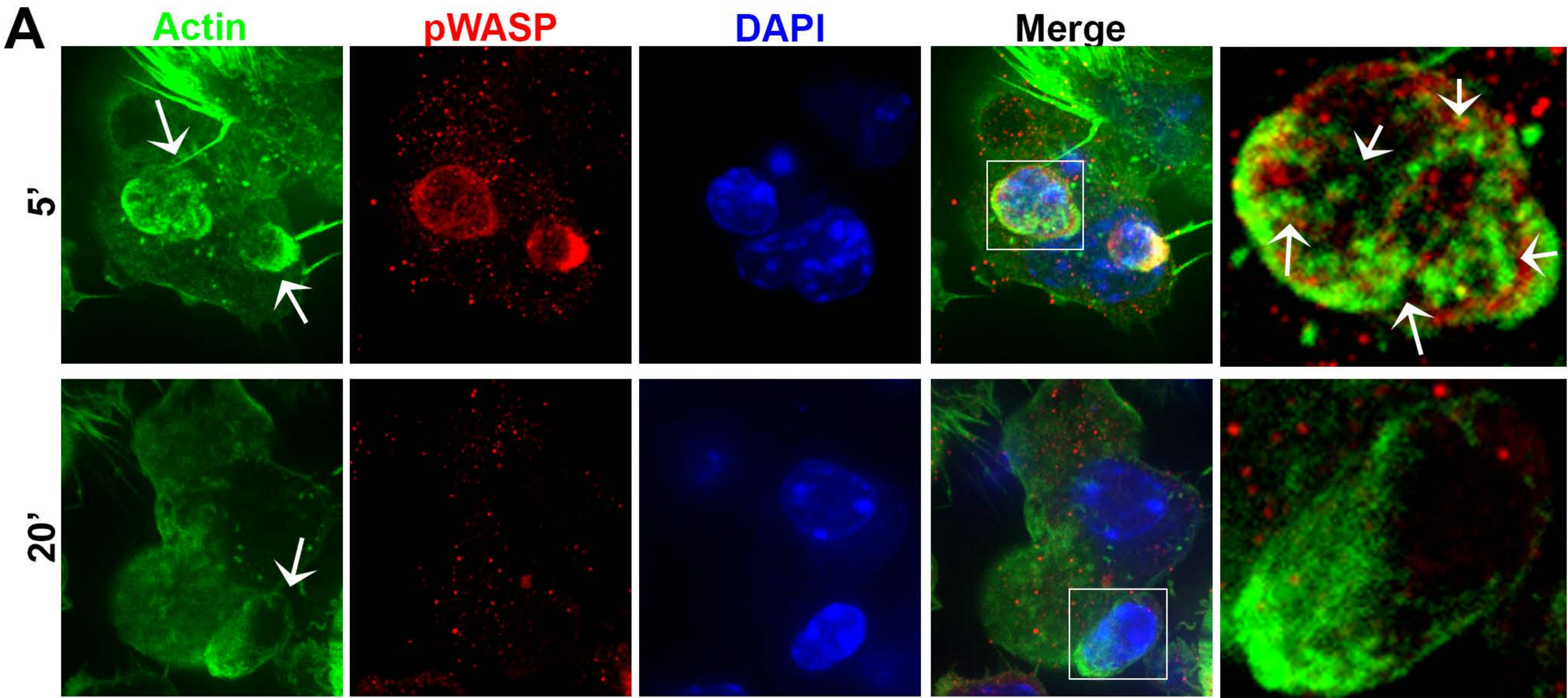


Figure S6

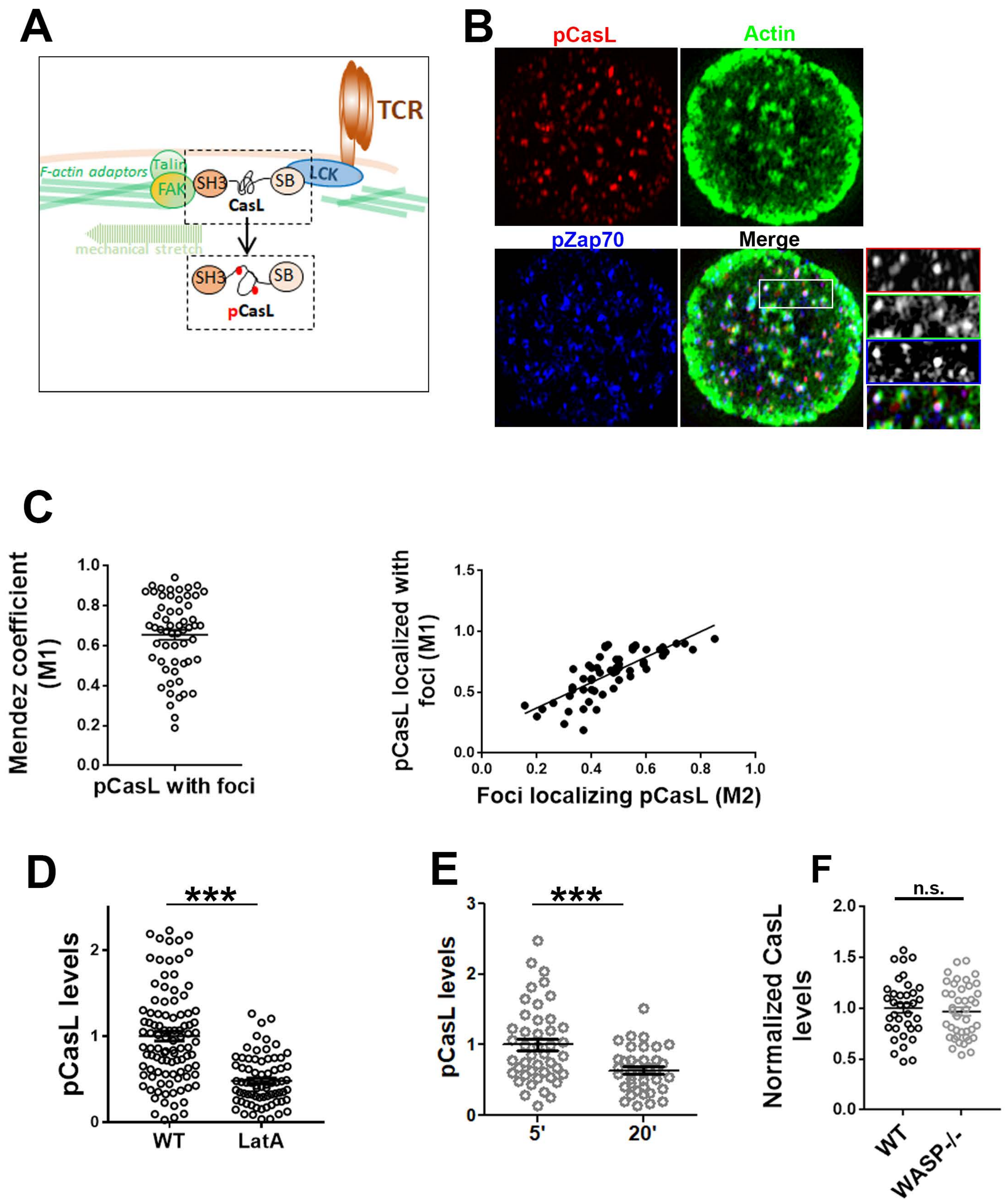


Figure S7

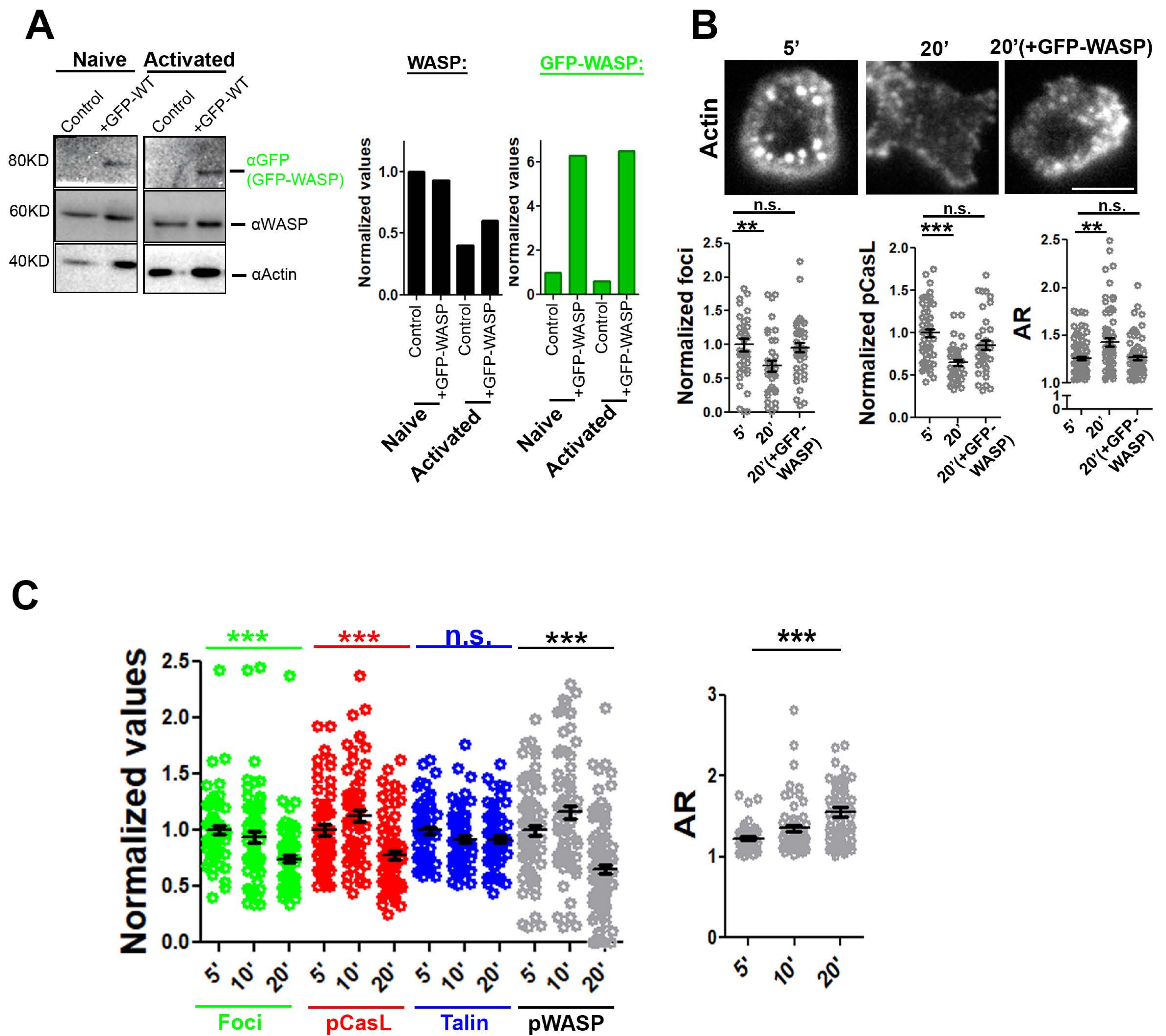


Figure S8

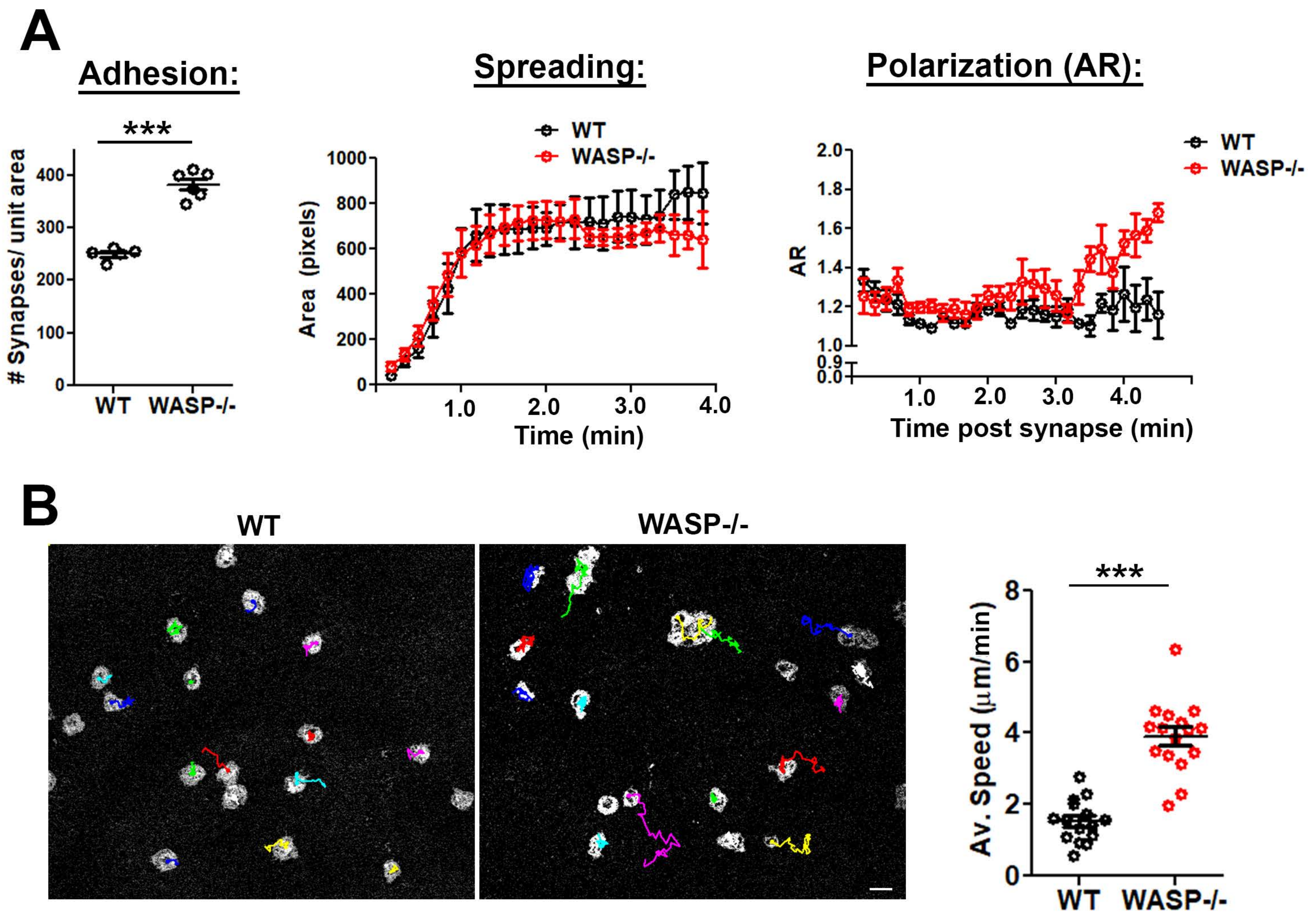


Figure S9

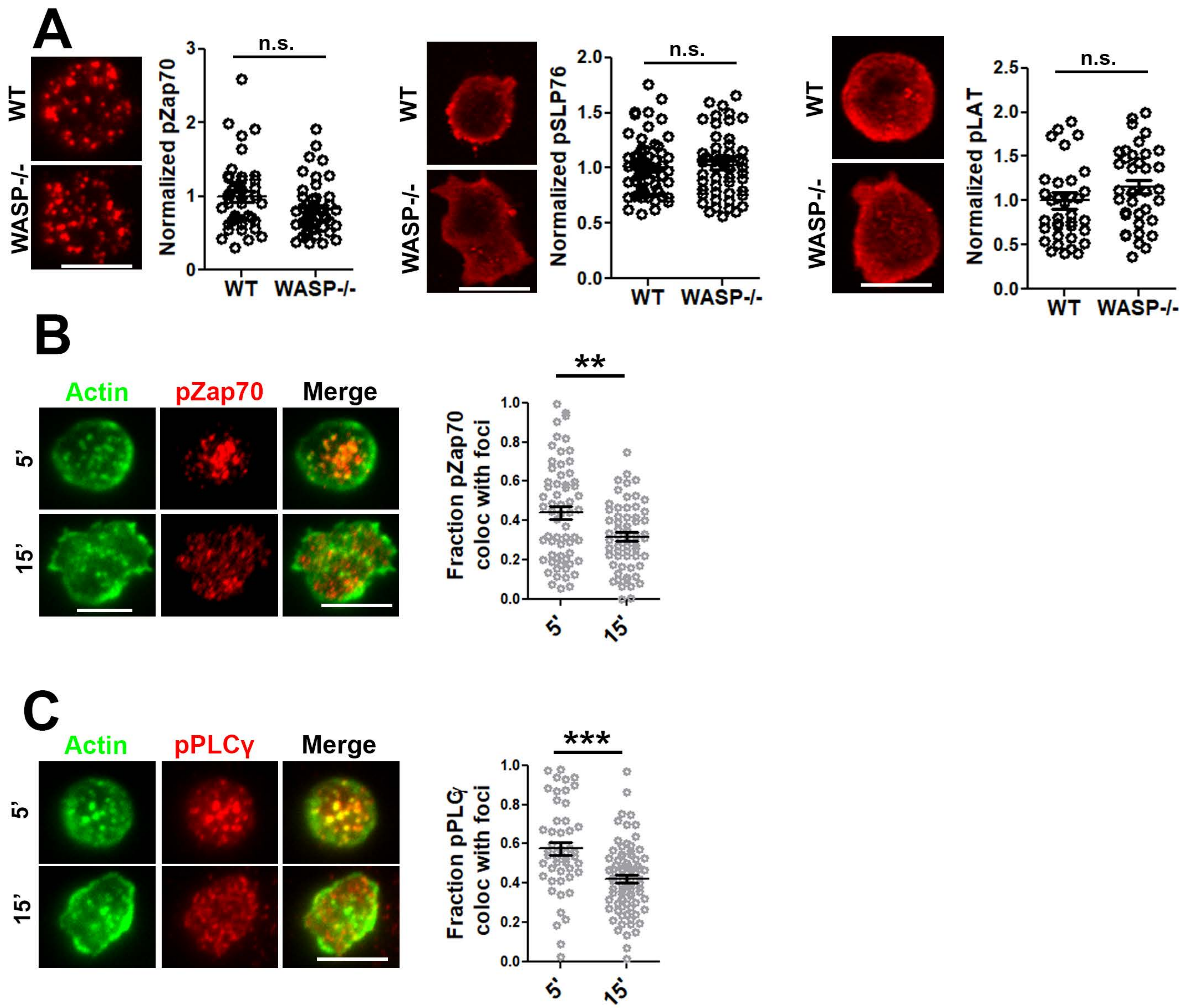
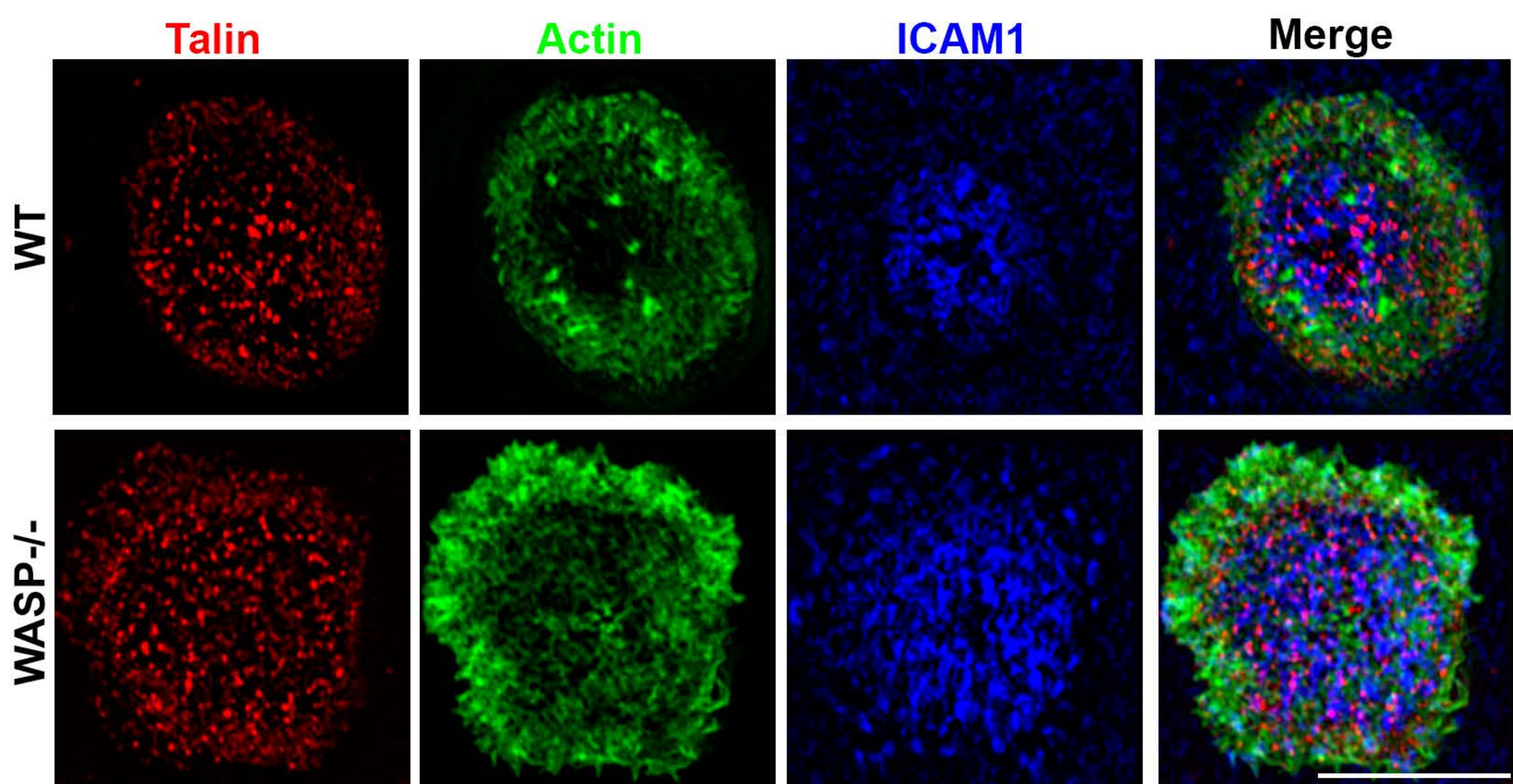


Figure S10

A



B

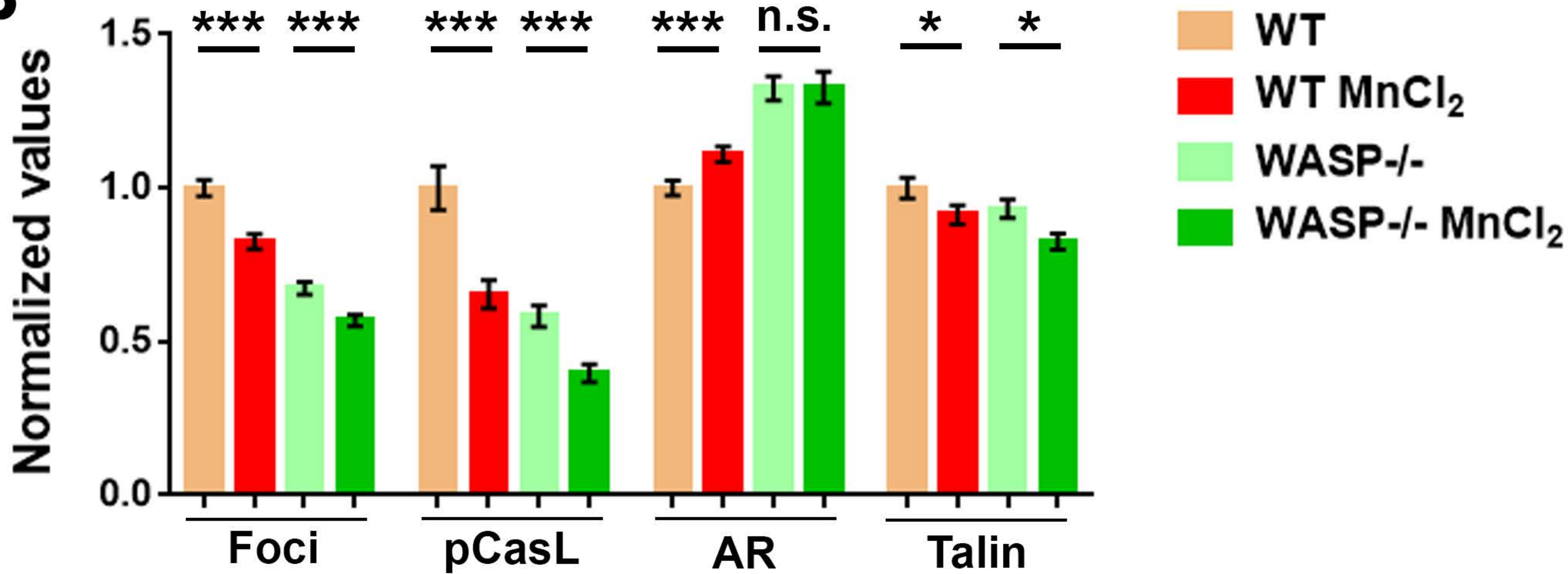
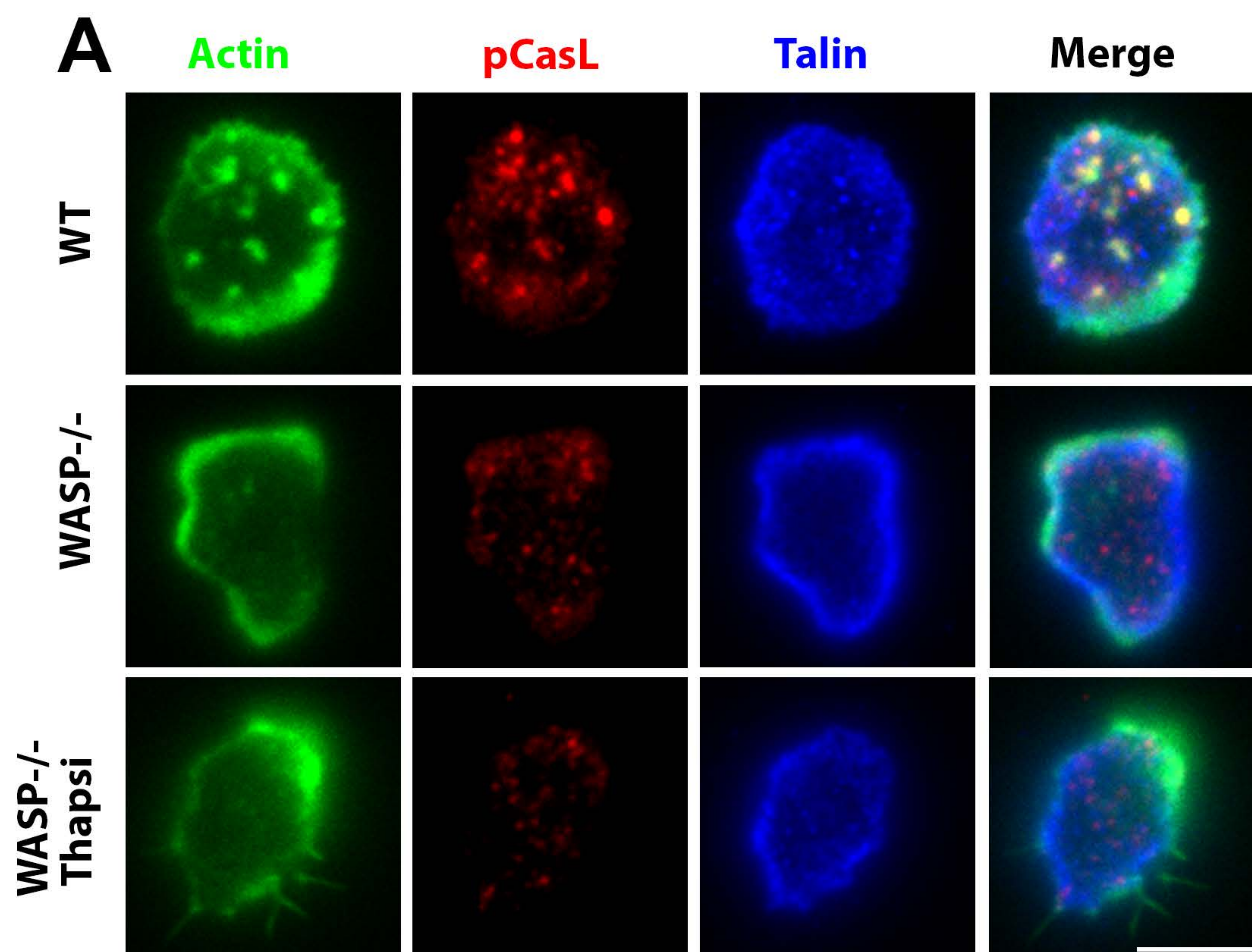


Figure S11



B

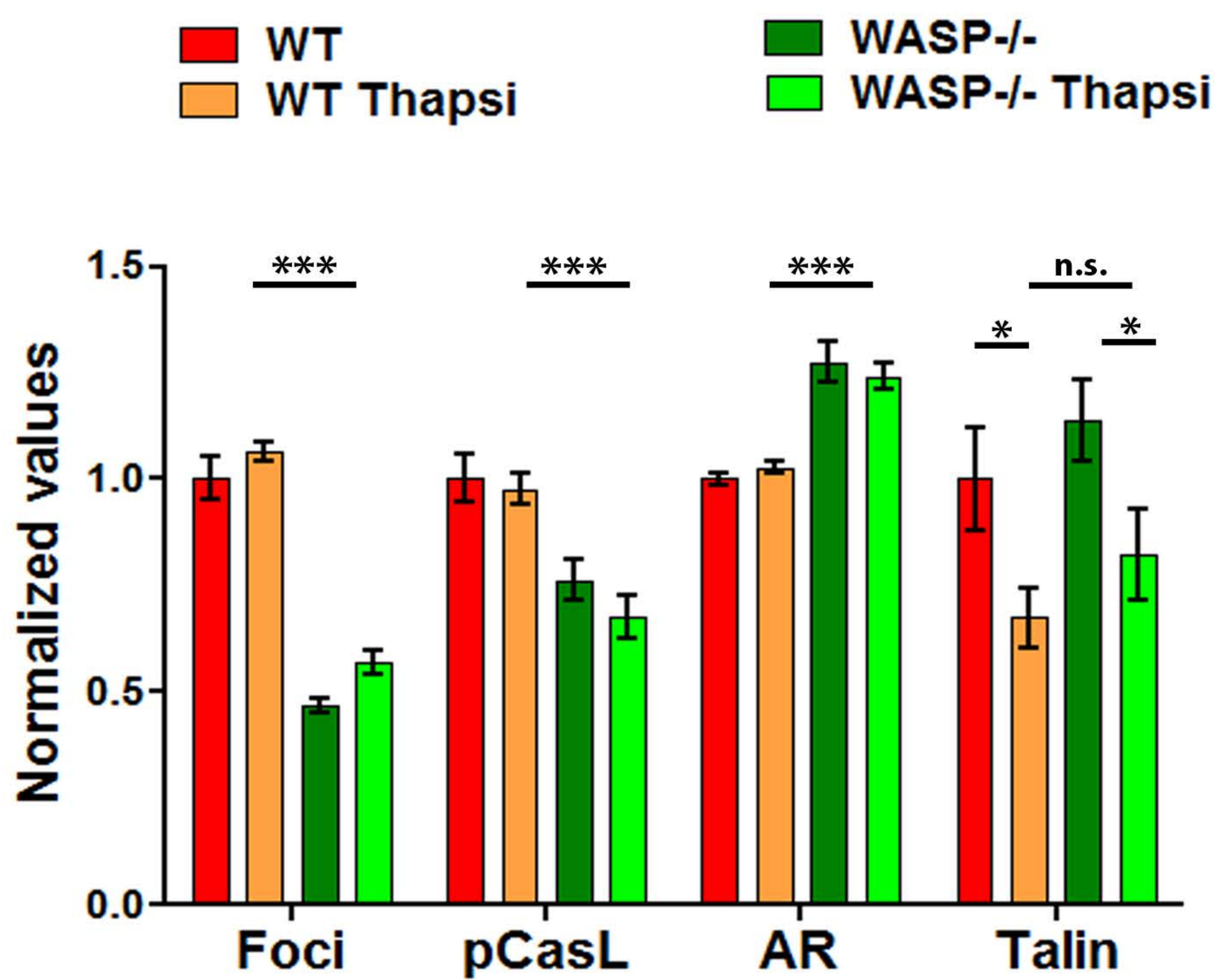


Figure S12

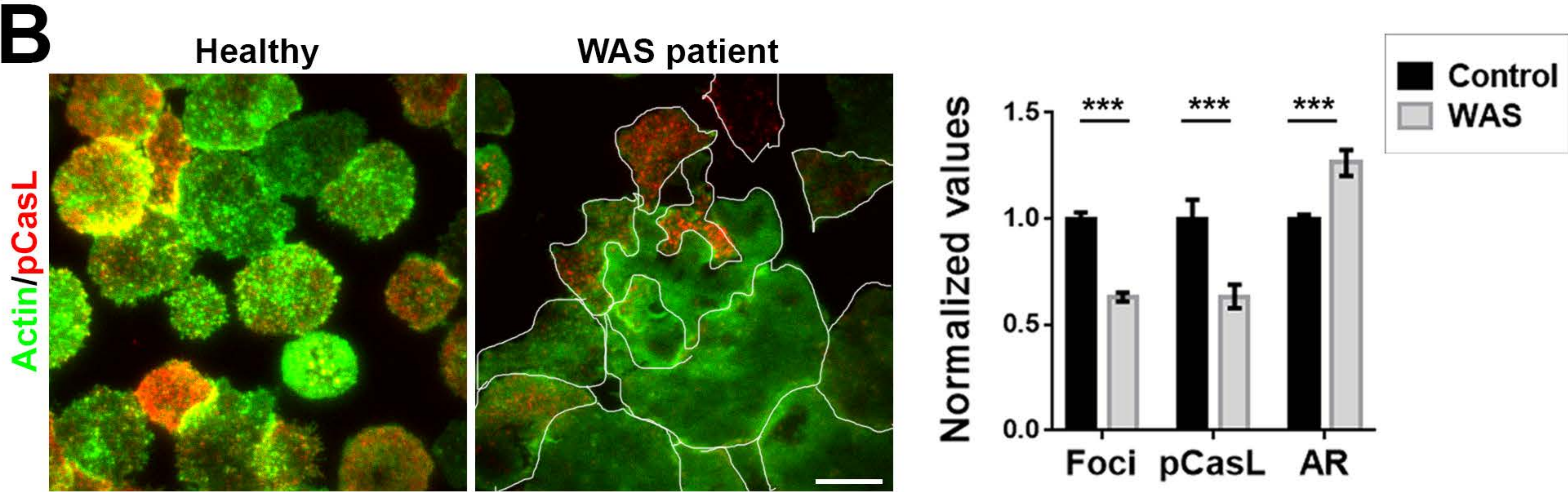
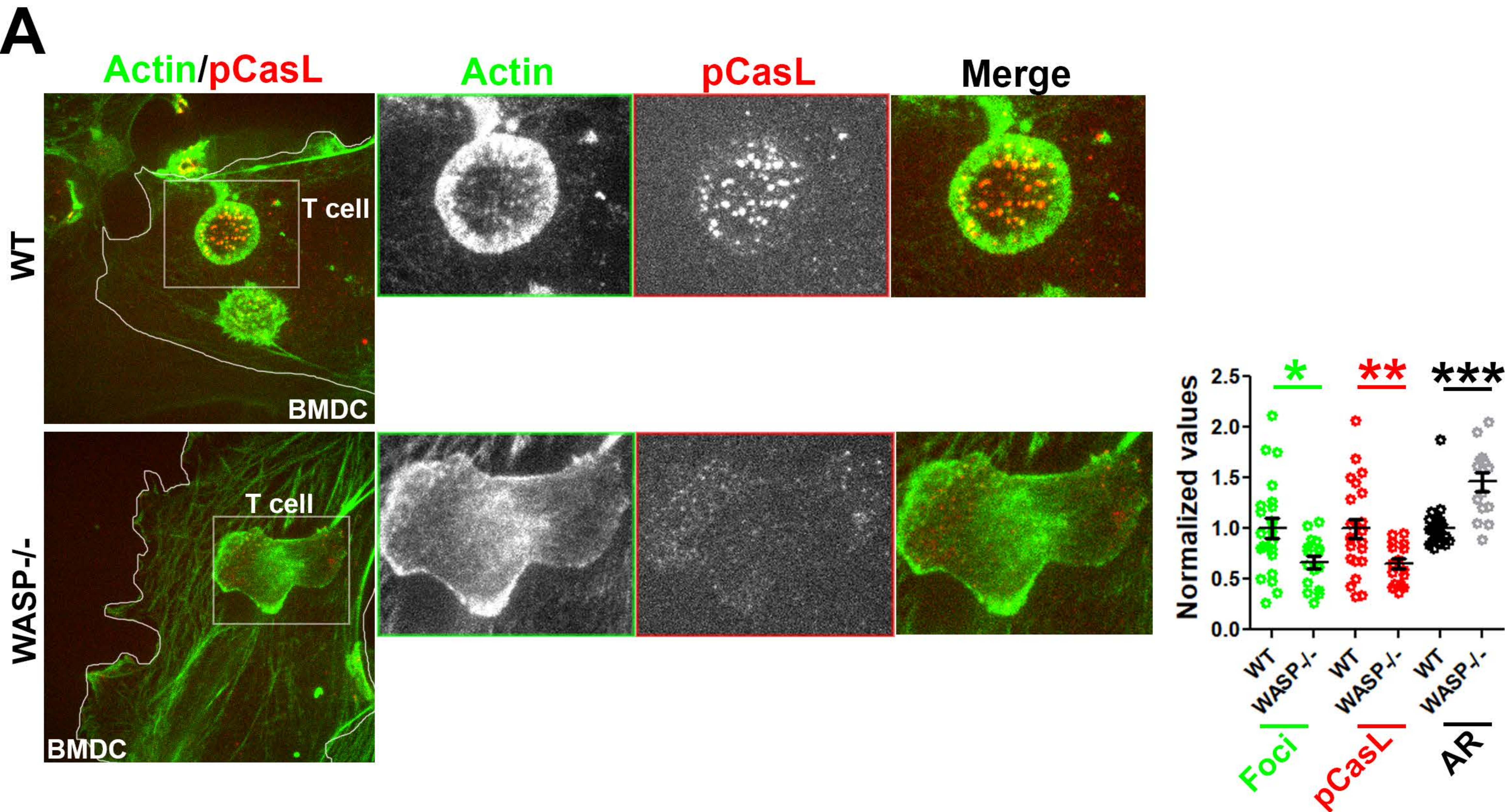


Figure S13

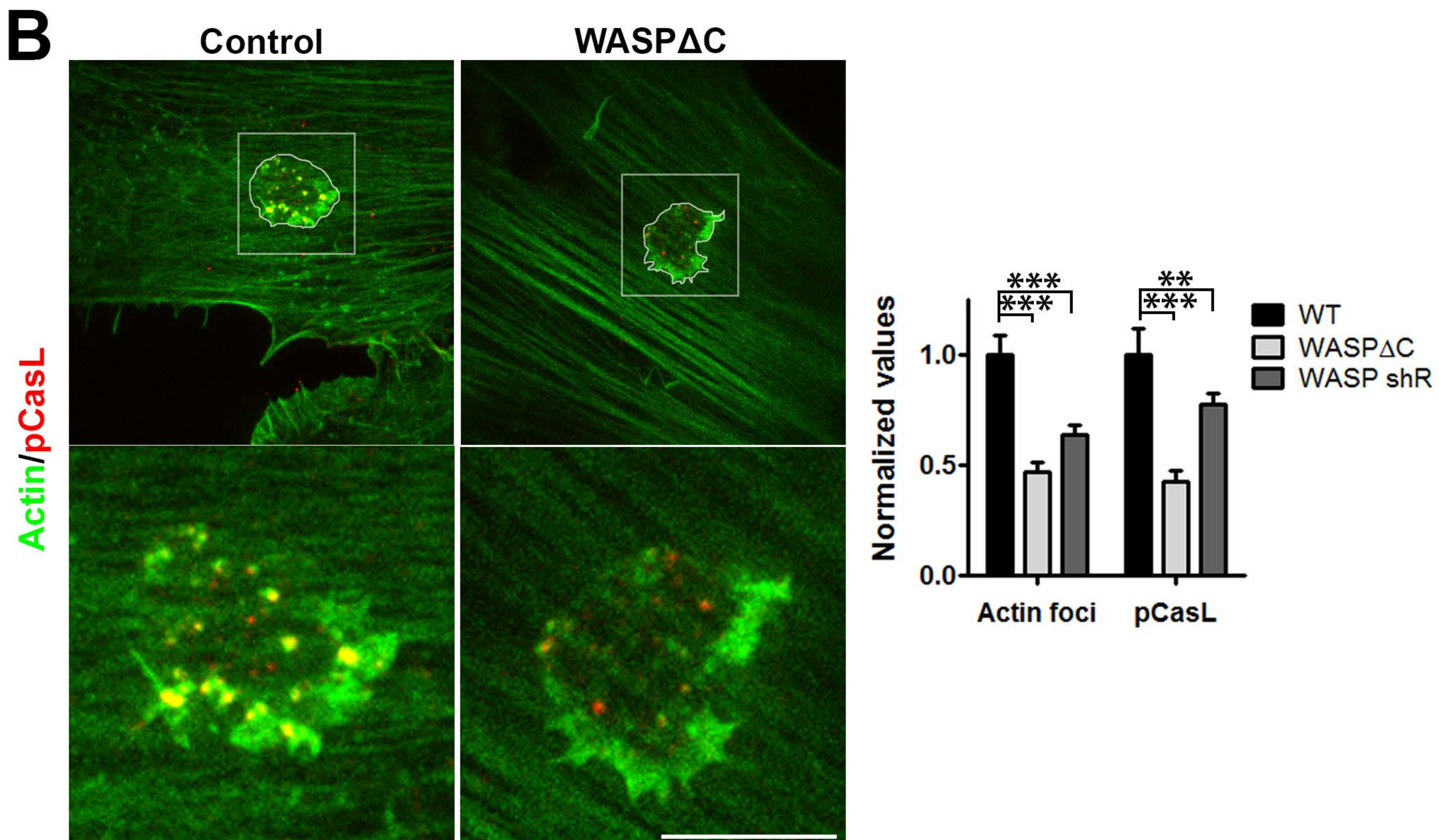
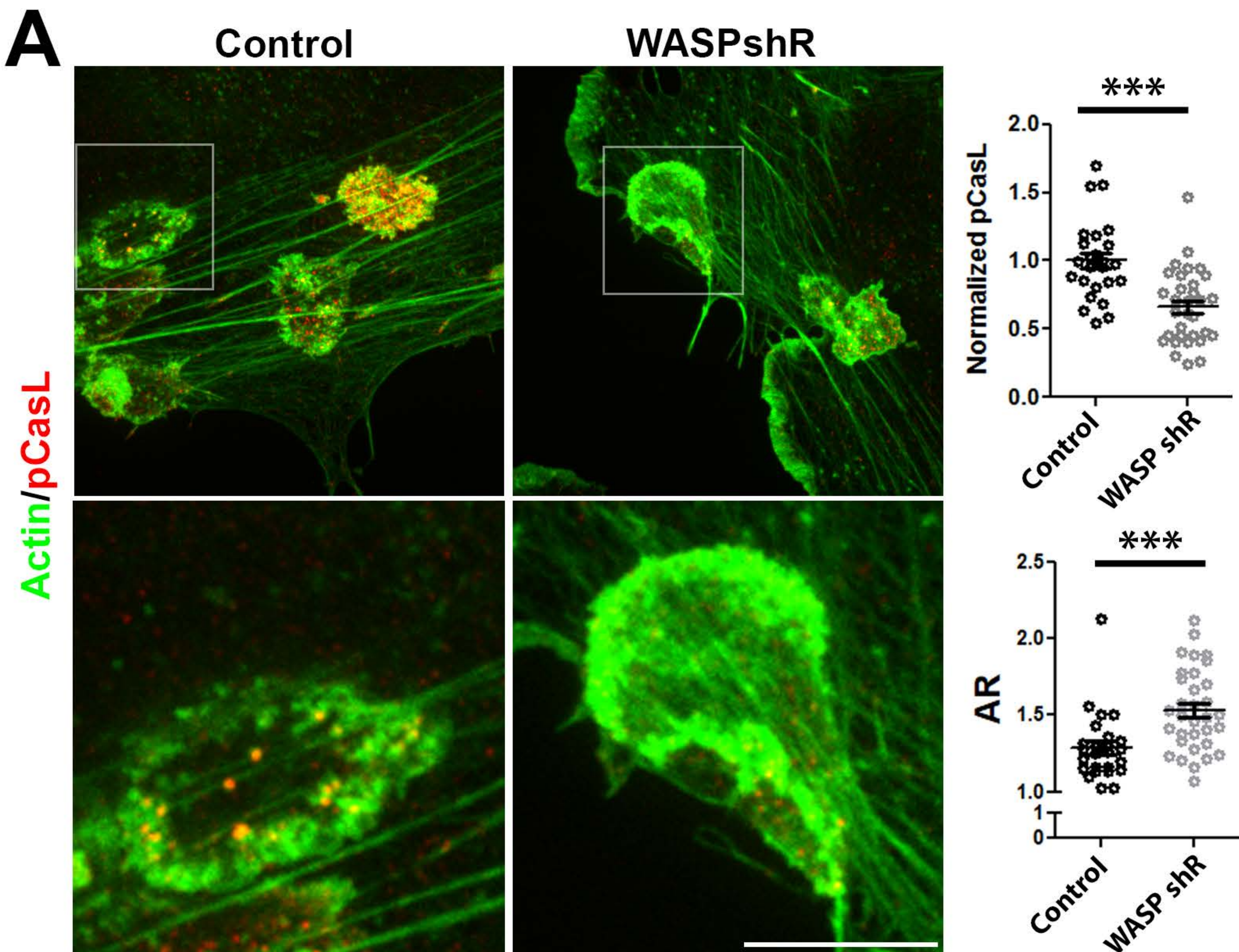


Figure S14

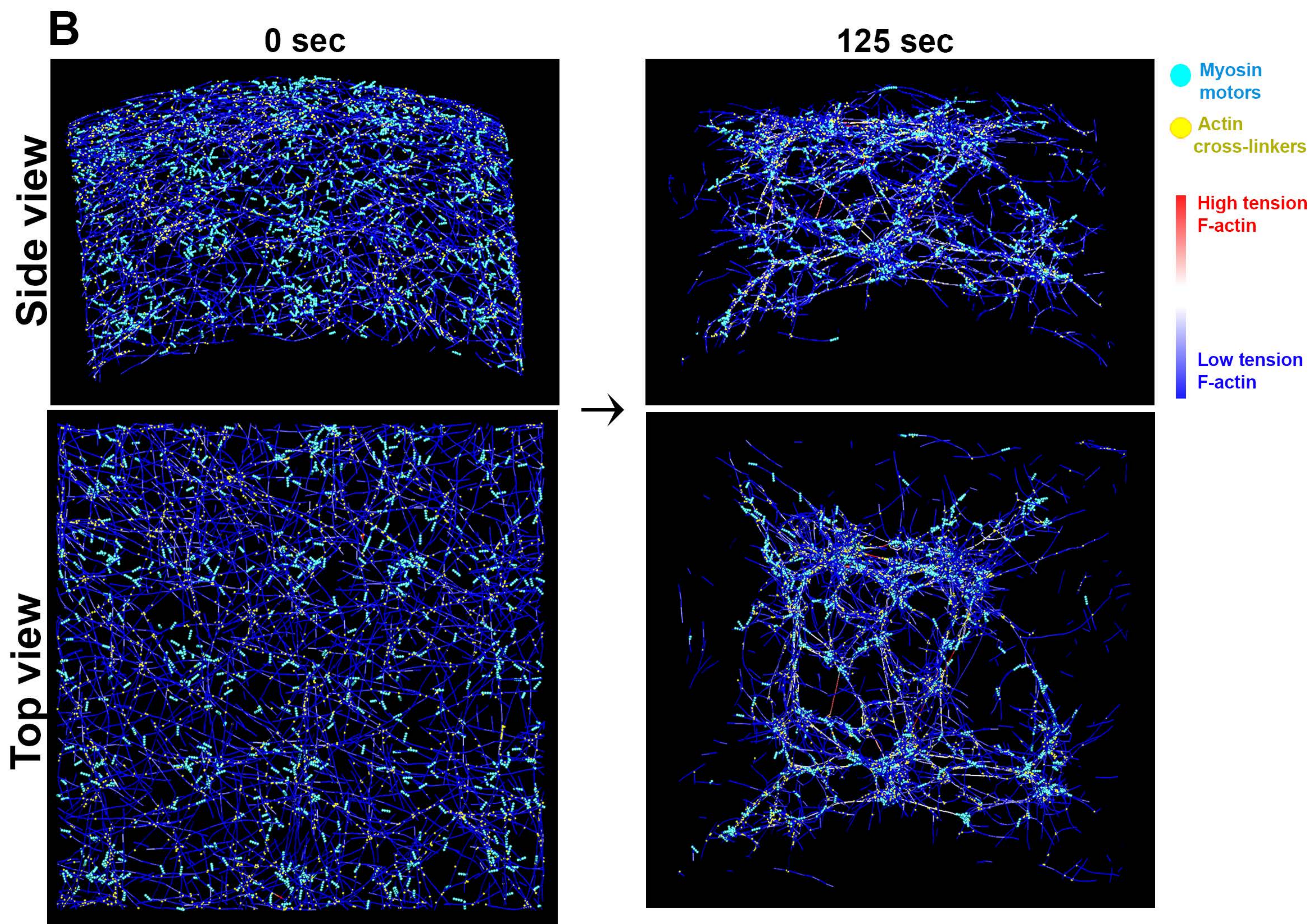
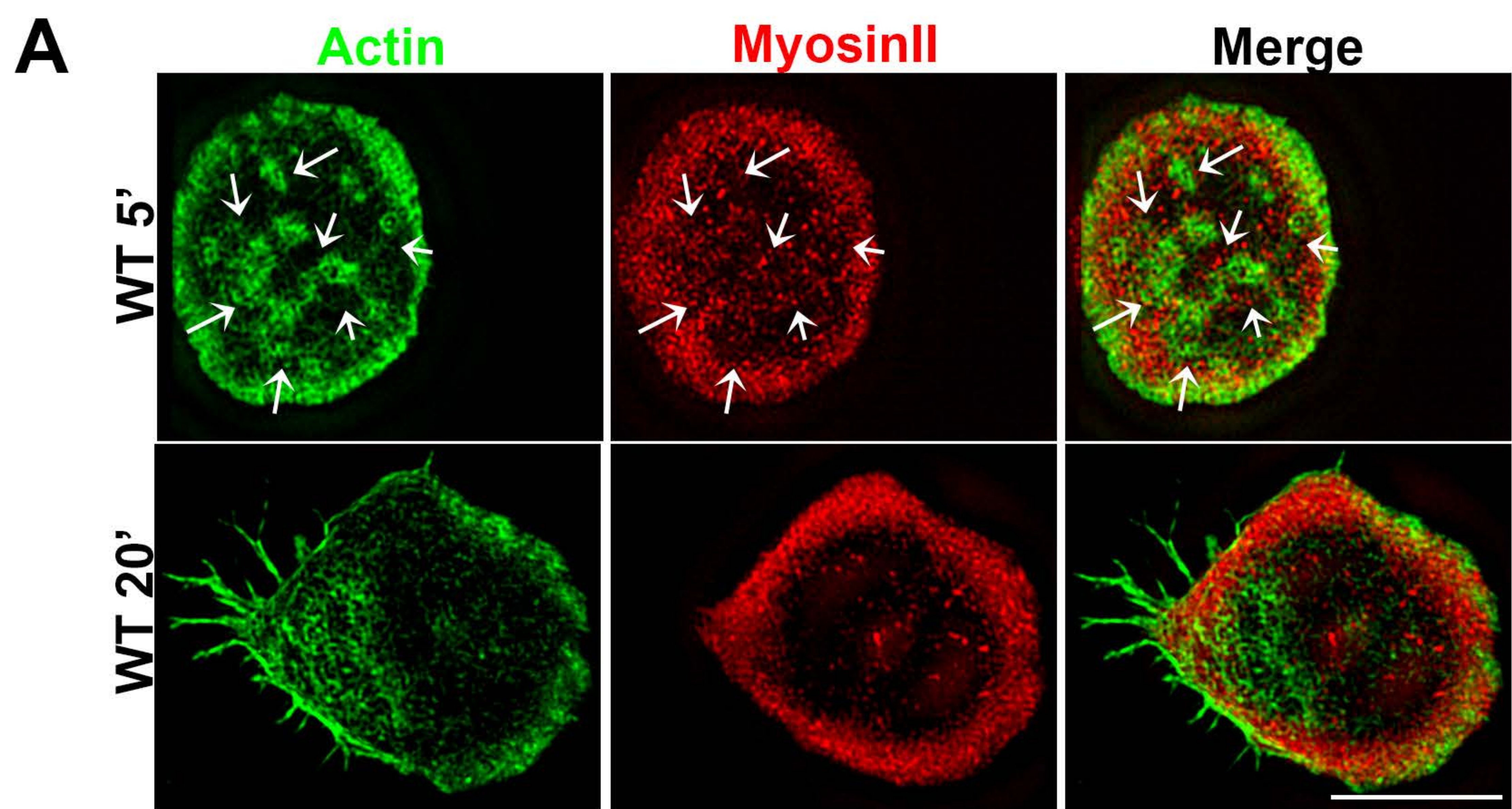


Figure S15

